

# Analytical Modeling of Cross-axis Coupling in Micromechanical Springs

Sitaraman Iyer,<sup>†</sup> Yong Zhou\* and Tamal Mukherjee<sup>†</sup>

<sup>†</sup>ECE Department, Carnegie Mellon University Pittsburgh, PA, 15213-3890

\*Advanced Micro Devices, Sunnyvale, CA 94088

## ABSTRACT

Analytical models to describe coupling between different directions of motion are derived using energy methods and verified for the U-spring, crab-leg spring and the serpentine spring. Finite element analyses (FEA) are done for a range of spring dimensions for each spring type in order to verify the models and determine the validity range. The models for the serpentine spring are then incorporated into a macromodel for use in nodal simulation. Improvement in simulation time using the macromodel over beam-based simulation is evaluated. Cross-axis coupling in an accelerometer structure is also simulated using this macromodel.

**Keywords:** Modeling, cross-axis coupling, micromechanical springs, lumped parameter modeling

## INTRODUCTION

Over the past few years a number of micromachined accelerometer and gyroscope designs have been published [1]. For these designs to be commercially viable, it is imperative to characterize their inherent non-idealities. Non-idealities in these devices including offset bias, cross-axis sensitivity and non-linearity occur due to a combination of undesired mechanical oscillation modes and mismatched sensing capacitances [2]. Undesired oscillation modes are caused by inherent cross-axis coupling in the suspension springs. In order to understand and predict the non-idealities, models for the cross-axis coupling in springs need to be derived.

A number of inertial sensors mentioned in [1] are made up of a mechanical proof-mass suspended by four springs. Each spring can be represented by a 6X6 lumped-element stiffness matrix (Figure 1). The overall system stiffness matrix is obtained as a summation of the individual stiffness matrices. When all the four spring geometries are identical, and the layout is two-fold symmetric, the system stiffness matrix is diagonal because the cross-axis (off-diagonal) terms cancel out. However, due to manufacturing variations, the springs are not perfectly matched leading to a non-diagonal stiffness matrix. This causes the eigenmodes of the system to deviate from the principal axes and results in elliptical motion of the proof-mass instead of the expected straight line motion [3].

In [4], non-linear rod theory has been applied to analyze the vibration modes of a MEMS gyroscope considering the modes to be uncoupled. Coupling among three specific modes of a gyroscope structure has been investigated in [5].

Shaded elements are zero

$$K = \begin{bmatrix} k_{xx} & k_{xy} & k_{xz} & k_{x\theta_x} & k_{y\theta_y} & k_{x\theta_z} \\ k_{yx} & k_{yy} & k_{yz} & k_{y\theta_x} & k_{y\theta_y} & k_{y\theta_z} \\ k_{zx} & k_{zy} & k_{zz} & k_{z\theta_x} & k_{z\theta_y} & k_{z\theta_z} \\ k_{\theta_{xx}} & k_{\theta_{xy}} & k_{\theta_{xz}} & k_{\theta_{x\theta_x}} & k_{\theta_{x\theta_y}} & k_{\theta_{x\theta_z}} \\ k_{\theta_{yx}} & k_{\theta_{yy}} & k_{\theta_{yz}} & k_{\theta_{y\theta_x}} & k_{\theta_{y\theta_y}} & k_{\theta_{y\theta_z}} \\ k_{\theta_{zx}} & k_{\theta_{zy}} & k_{\theta_{zz}} & k_{\theta_{z\theta_x}} & k_{\theta_{z\theta_y}} & k_{\theta_{z\theta_z}} \end{bmatrix}$$

FIGURE 1. Elements of the stiffness matrix. This symmetric matrix has 21 distinct terms. The number of distinct non-zero terms reduces to 12 assuming there is no variation in geometry along the  $z$  direction and therefore, no coupling between in-plane and out-of-plane directions.

In this paper it is our aim to model the coupling between the principal modes of a suspended structure by deriving linear models for three widely used types of suspension springs.

The modeling approach is presented first, followed by verification of these models using FEA. Then, the results of the nodal simulation using the serpentine spring macromodel are discussed.

## MODELING

The three types of springs are parameterized as shown in Figure 2. Linear equations for the spring constants are derived using energy methods. A force (or moment) is applied to the free end(s) of the spring, in the direction of interest, and the displacement is calculated symbolically (as a function of the design variables and the applied force). In these calculations different boundary conditions are applied for the different modes of deformation of the spring.

When forces (moments) are applied at the end-points of the flexure, the total energy of deformation,  $U$ , is calculated as:

$$U = \sum_{beam\ i=1}^N \int_0^{L_i} \frac{M_i(\xi)^2}{2EI_i} d\xi \quad (1)$$

where,  $L_i$  is the length of the  $i$ 'th beam in the flexure,  $M_i$  is the bending moment transmitted through beam  $i$ ,  $E$  is the Young's modulus of the structural material and  $I_i$  is the moment of inertia of beam  $i$ , about the relevant axis. The bending moment is a linear function of the forces and moments applied to the end-points of the flexure. The dis-

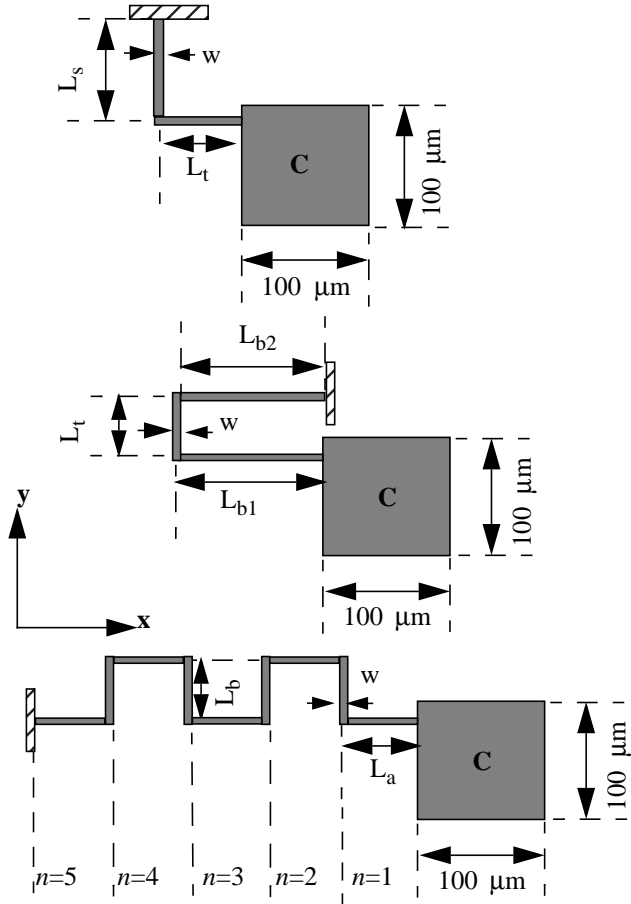


FIGURE 2. Design variables for crab-leg-spring, U-spring and serpentine spring with proof-mass. The external forces and moments are applied at C, the centroid of the plate mass, with only one spring in the analysis so that all the cross-axis terms can be clearly observed.

placement of an end-point of the flexure in any direction  $\zeta$  is given as:

$$\delta\zeta = \frac{\partial U}{\partial F_\zeta} \quad (2)$$

where,  $F_\zeta$  is the force applied in that direction at that end point [6]. Similarly, angular displacements can be related to applied moments.

The models for three diagonal elements (*i.e.*, the translational spring constants) have been derived previously [7]. Our aim here is to obtain the displacement in a direction as a function of the applied force (moment) in some other direction. Applying the boundary conditions, as shown in Figure 3 and Table I, we obtain a set of linear equations in terms of the applied forces and moments and the unknown displacement. Solving the set of equations yields a linear relationship between the displacement and applied force for the cross-axis spring constant of interest [7]. The constant of

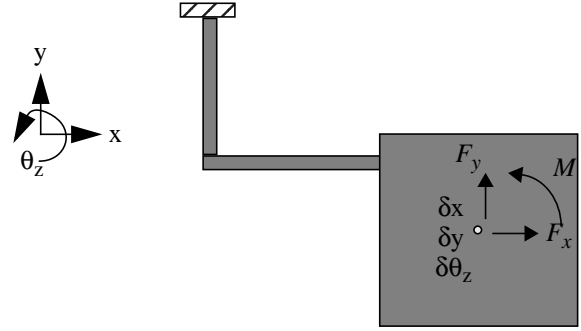


FIGURE 3. Forces and moments applied at the centroid of a proof-mass attached to the free end of a crab-leg. Boundary conditions are applied as equality constraints on the three displacements.

Table I Boundary conditions and equations to be solved for calculating spring constants

Spring constant	Boundary conditions	Force/Moment to be solved for
$k_{xy}$	$\delta x = 0, \delta\theta_z = 0$	$F_x$
$k_{x\theta_z}$	$\delta x = 0, \delta y = 0$	$F_x$
$k_{y\theta_z}$	$\delta x = 0, \delta y = 0$	$F_y$

proportionality gives the spring constant as a function of the physical dimensions of the spring. The models for the out-of-plane cross-axis spring constants are similarly derived.

For the crab-leg, the analytical model for coupling between  $x$  and  $y$  directions for one spring is:

$$k_{xy} = \frac{9EI_t I_s}{L_t L_s (I_t L_s + I_s L_t)} \text{ where, } I_t \text{ and } I_s \text{ are the moments}$$

of inertia of the crab-leg-beams.

For one U-spring, assuming  $L_{b1} \sim L_{b2}$  and  $L_t \ll L_{b1}$ , the derived analytical model is simplified to get:

$$k_{xy} = \frac{3EI_t(L_{b1} - L_{b2})}{L_t L_{b1}^3}, \text{ where } I_t \text{ is the moment of inertia}$$

of the U-spring connecting truss and  $E$  is the Young's Modulus of the beam material. For a serpentine spring the  $k_{xy}$  for even  $n$  is given in (3) and for odd  $n$   $k_{xy} = 0$ .

The above models are for a single spring. These models suggest design directions for reducing  $k_{xy}$ , and thereby, the device non-idealities. It is possible to eliminate the nominal system  $k_{xy}$  by symmetrically placing four springs. Manufacturing variations are commonly modeled as functions of wafer position, implying that closely placed beams (as in the same spring) have less width variation than beams which are farther apart (like those on two different springs). In addi-

$$k_{xy-serpentine} = \frac{(36EI_a I_b^2)}{(L_b)(L_b^2 I_a^2 (n-2)(n-1)^2 + 3L_a^2 I_b^2 n(n^2-3) + 2L_a L_b I_a I_b n(2n^2-5n+3))} \quad (3)$$

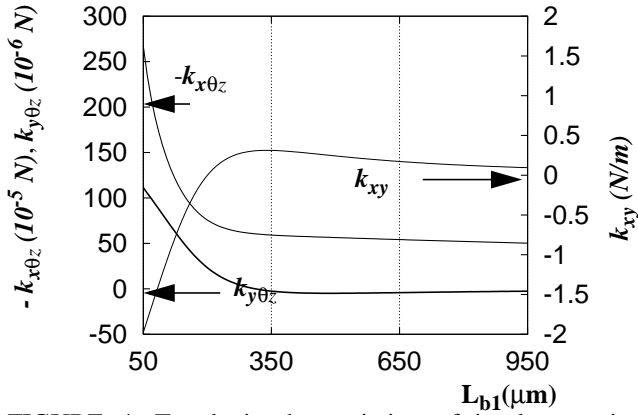


FIGURE 4. Trends in the variation of in-plane spring constants for the U-spring for varying beam lengths ( $L_{b1}$ ). The design variables are set to:  $w=2.0 \mu\text{m}$ ,  $L_t=10.0 \mu\text{m}$ ,  $L_{b2}=200.0 \mu\text{m}$

tion to eliminating nominal system  $k_{xy}$ , long range width variations can also be nullified by designing the two beams with equal lengths and widths for a U-spring or by choosing  $n$  to be odd for a serpentine spring. In Figure 4 it is seen that it is possible to design the U-spring such that the values of  $k_{xy}$  and  $k_{x\theta z}$  are very small. Similar trends for the serpentine spring are shown in Figure 5.

### MODEL VERIFICATION

The models derived above are compared to FEA results. There are three design variables for the crab-leg, four for the U-spring and four for the serpentine spring. A convergence analysis was done to determine the granularity of the finite element mesh that was required. Consequently, each beam was split into 40 divisions along the length and 10 divisions along the width. FEA with 3D quadratic brick elements was done on 8 crab-leg designs, 16 U-spring designs and 8 serpentine spring designs. For the crab-leg spring and the U-spring it was seen from the FEA results that, for beam widths of  $2 \mu\text{m}$ , when the beam lengths are at

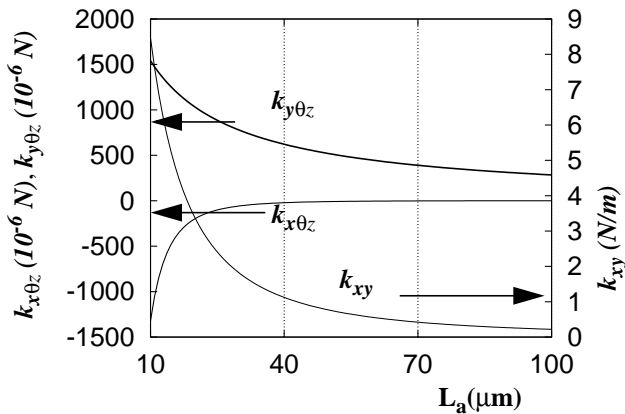


FIGURE 5. Trends in the variation of in-plane spring constants for the serpentine-spring for varying beam lengths ( $a$ ). The design variables are set to:  $w=2.0 \mu\text{m}$ ,  $L_b=20.0 \mu\text{m}$ ,  $n=4$ .

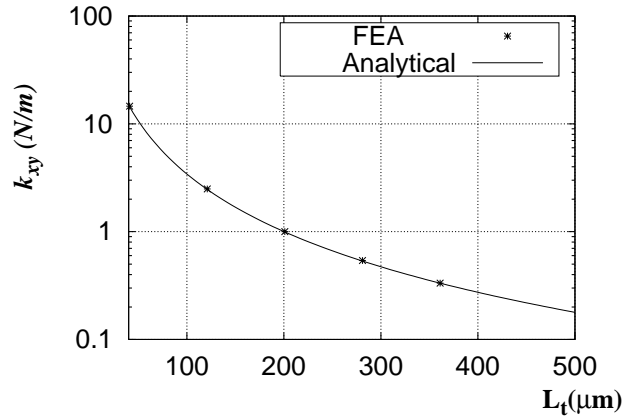


FIGURE 6. Comparison of analytical model and FEA for crab-leg-spring  $k_{xy}$  for varying crab-leg thigh lengths ( $L_t$ ). The design variables are set to:  $w=2.0 \mu\text{m}$ ,  $L_s=50.0 \mu\text{m}$

least 0.75 times the mass dimensions, all the models match the FEA values to within 10%. For smaller beam lengths the mass ceases to be rigid. Mass deformations are not considered in this spring modeling exercise. For the serpentine spring it was not possible to obtain accurate values of  $k_{xy}$  from FEA when the values were low. All the models other than  $k_{y\theta z}$  match FEA results to within 10% for beam widths of  $2 \mu\text{m}$ . The  $k_{y\theta z}$  also matches within 10% except when  $L_b$  is much greater than  $L_a$ .

Further, keeping all other design variables constant, the variation of  $k_{xy}$  with the beam length was studied. As seen in Figure 6, Figure 7 and Figure 8 respectively the analytical models match the FEA values to within 2% for the crab-leg, 5% for the U-spring and 9% for the serpentine-spring.

### ACCELEROMETER SIMULATION

A macromodel for the serpentine spring was incorporated in NODAS, a nodal simulator for microelectromechanical systems [8][9]. AC analysis of a proof-mass

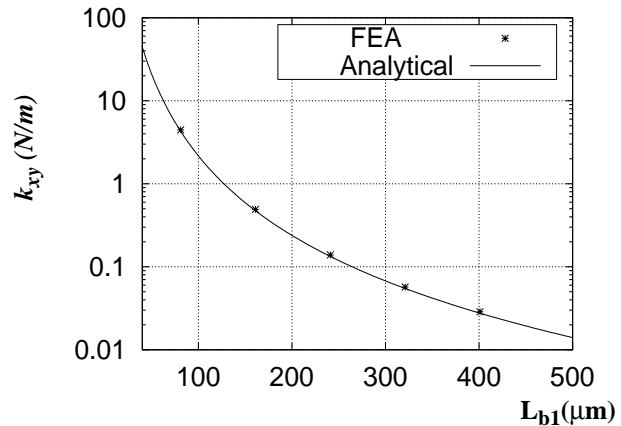


FIGURE 7. Comparison of analytical model and FEA for U-spring  $k_{xy}$  for varying U-spring beam lengths ( $L_{b1}$ ). The design variables are set to:  $w=2.0 \mu\text{m}$ ,  $L_t=10.0 \mu\text{m}$ ,  $L_{b2}=L_{b1}-30.0 \mu\text{m}$

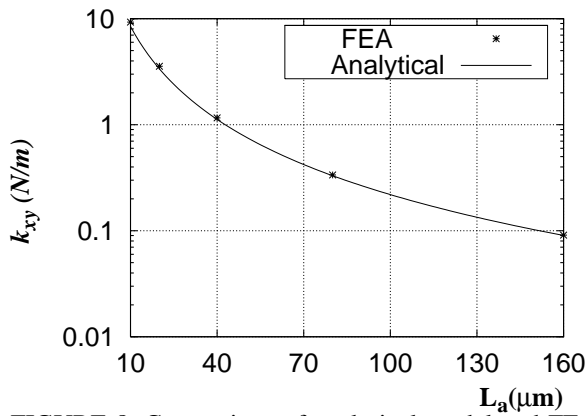


FIGURE 8. Comparison of analytical model and FEA for serpentine-spring  $k_{xy}$  for varying serpentine-spring beam lengths (a). The design variables are set to:  $w=2.0 \mu\text{m}$ ,  $L_b=20.0 \mu\text{m}$ ,  $n=4$

suspended by four serpentine springs was done using the spring macromodel as well as individual beam elements. The macromodel-based simulation (with  $n=4$ ) was about 5 times faster than the individual beam element-based simulation. For higher  $n$ , the speedup will be greater.

The serpentine spring, proof-mass structure described above was employed as a  $y$ -accelerometer. Input accelerations were applied in both the  $x$  and the  $y$  directions. Mode coupling is observed in FEA when diagonal springs are identical and one pair of diagonal springs is wider than the other pair. This configuration was simulated using the serpentine spring macromodel in NODAS. As expected, a significant cross-axis sensitivity (resulting from mode coupling) is seen in the  $V_{out}$  waveform in Figure 9.

## CONCLUSIONS

Analytical models are derived for the spring stiffness matrix for the U-spring, crab-leg spring and the serpentine

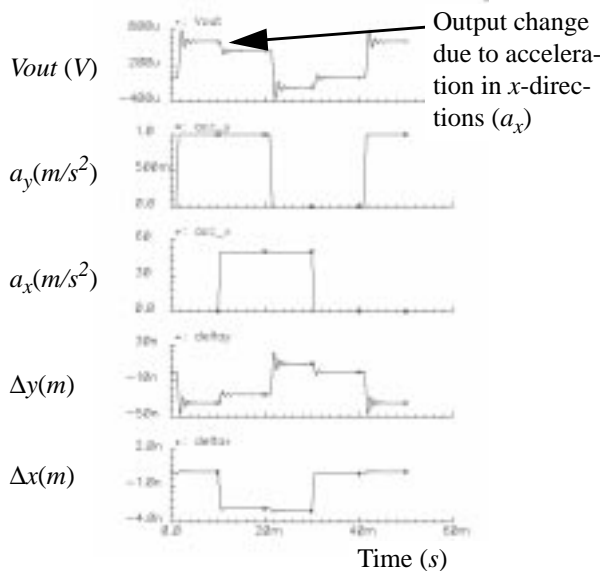


FIGURE 9. NODAS simulation of cross-axis sensitivity in  $y$ -accelerometer

spring. From comparison with FEA it is seen that these models are accurate to within 10% over a range of values of the design variables. These models are intended to be used for understanding and modeling more complex effects such as beam width-mismatch caused by manufacturing variations. Higher level macromodels enable iterative designing of inertial sensors by allowing rapid evaluation of performance criteria such as cross-axis sensitivity. They can also be embedded into synthesis tools for faster evaluation of candidate designs. Simple pointers (for instance, equate U-spring beam lengths or use serpentine springs with odd  $n$  to eliminate  $k_{xy}$ ) to aid MEMS designers can be deduced from the model equations.

## ACKNOWLEDGEMENTS

The authors thank Qi Jing and Bikram Baidya for their help in NODAS. This research effort is sponsored by the Defence Advanced Research Projects Agency (DARPA) and U. S. Air Force Research Laboratory, under agreement number F30602-96-2-0304. The U.S. Government is authorized to reproduce and distribute reprints for governmental purposes notwithstanding any copyright notation thereon. The views and conclusions contained herein are those of the authors and should not be interpreted as necessarily representing the official policies or endorsements, either expressed or implied, of DARPA, the U. S. Air Force Research Laboratory, or the U. S. Government.

## REFERENCES

- [1] N. Yazdi, F. Ayazi, and K. Najafi, "Micromachined Inertial Sensors", *Proc. IEEE*, vol. 86, no. 8, pp. 1640-1659, Aug 1998
- [2] T. Mukherjee, Y. Zhou, and G. K. Fedder, "Automated Optimal Synthesis of Microaccelerometers", *Proc. IEEE MEMS '99*, Orlando, Florida, January 1999, pp. 326-331
- [3] Y. Mochida, M. Tamura, and K. Ohwada, "A Micromachined Vibrating Rate Gyroscope with Independent Beams for the Drive and Detection Modes", *Proc. MEMS '99*, Orlando, Florida, January 1999, pp. 618-623
- [4] W. O. Davis, and A. P. Pisano, "On the Vibrations of a MEMS Gyroscope," *Proc. MSM '98*, Santa Clara, CA, pp. 557-562, April 6-8 1998
- [5] Y. Ansel, Ph. Lerch, and Ph. Renaud, "Mode coupling aspects in a vibrating gyroscope," *Sensors and Actuators A* 62, pp. 576-581, 1997
- [6] J. M. Gere and S. P. Timoshenko, *Mechanics of Materials*, PWS Publishing Company, Boston, 4th edition, 1997.
- [7] G. K. Fedder, "Simulation of Microelectromechanical Systems", *Ph. D. Thesis*, EECS Department, University of California at Berkeley, September 1994.
- [8] J. Vandemeer, M. S. Kranz, and G. K. Fedder, "Hierarchical Representation and Simulation of Micromachined Inertial Sensors," *Proc. MSM '98*, Santa Clara, CA, pp. 540-545, April 6-8 1998
- [9] G. K. Fedder and Q. Jing, "A Hierarchical Circuit-Level Design Methodology for Microelectromechanical Systems," *IEEE Trans. Circuits and Systems*, (To be published)